ACS Catalysis

Research Article

pubs.acs.org/acscatalysis

Confinement Effects in Lewis Acid-Catalyzed Sugar Conversion: Steering Toward Functional Polyester Building Blocks

Rik De Clercq,[†] Michiel Dusselier,*[,†,§] Charles Christiaens,[†] Jan Dijkmans,[†] Remus Ion Iacobescu,[‡] Yiannis Pontikes,[‡] and Bert F. Sels*[,†]

[†]Center for Surface Chemistry and Catalysis, KU Leuven, Kasteelpark Arenberg 23, 3001 Leuven, Belgium

[‡]Department of Materials Science, KU Leuven, Kasteelpark Arenberg 44, 3001 Leuven, Belgium

Supporting Information

ABSTRACT: We report the use of solid Lewis acid catalysts for the conversion of tetrose sugars to four-carbon α-hydroxy acid esters (C_4-AHA), which are useful as functional polyester building blocks. Sn-β was by far the most active and selective catalyst, yielding up to 80% methyl vinyl glycolate (MVG), methyl-4-methoxy-2-hydroxybutanoate (MMHB), and α-hydroxy-γ-butyrolactone (HBL) combined at 95% conversion. A very high turnover frequency (TOF) of 330 $mol_{C4\text{-}AHA}$ mol_{Sn} h^{-1} was attained using Sn-β, a more than 6-fold increase compared with homogeneous $SnCl_4{\cdot}5H_2O$. It is shown that, using different Sn-based catalysts with various pore sizes, the product distribution is strongly dependent on the size of the catalyst pores. Catalysts containing mainly mesopores, such as Sn-MCM-41 or Sn-SBA-15, prefer the production of the more bulky MMHB, whereas microporous catalysts such as Sn-β or Sn-MFI favor the production of MVG. This effect can be further enhanced by increasing the reaction temperature. At 363 K, only 20% MVG is attained using Sn-β, but at 433 K, this increases to 50%. Using a kinetic analysis, it was found that, in microporous catalysts, steric hindrance near the Sn active site in the catalyst pores plays a dominant role in favoring the reaction pathway toward MVG. Moreover, the selectivity toward both products is kinetically controlled.

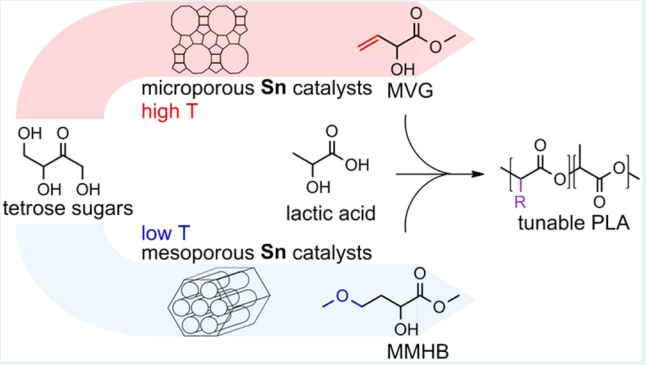

KEYWORDS: *solid Lewis acid, Sn-β, biomass conversion, α-hydroxy acids, polylactic acid (PLA), functional PLA, methyl vinyl glycolate, α-hydroxy-γ-butyrolactone*

INTRODUCTION

Solid Lewis acids have attracted a lot of attention because of their high catalytic activity in reactions such as the isomerization of carbohydrates;[1−10] Meerwein−Ponndorf−Verley reductions;[11−15] Baeyer−Villiger oxidations;[15−17] 1,2-hydride shifts;[18,19] and, more recently, aldol reactions.[20] One of the key reactions is the production of lactic acid or alkyl lactates from carbohydrates.[21−33] Lactic acid, a three-carbon (C_3) α-hydroxy acid, is considered one of the top carbohydrate-derived platform chemicals[34−36] because it is a precursor to a wide range of useful products, such as acrylic acid, pyruvic acid, propylene glycol, 2,3-pentanedione,[37−39] and green solvents.[40] Its most prominent use is as the renewable building block for the biodegradable plastic polylactic acid (PLA).[41,42] This polyester is considered a benign synthetic substitute for petrochemical-based plastics. The latter are usually nondegradable in nature, and this causes accumulation of plastic fragments in marine environments, even at remote locations.[43−47] PLA is of use in general applications such as packaging (foils, containers, ...), coatings, and fibers, as well as in biomedicine (in vivo sutures,[48] orthopedic devices,[49] and drug delivery[50]).

PLA suffers from a few limitations, however, which could hamper its use for particular applications.[51] More specifically, traditional, stereoregular L-PLA is very brittle and relatively (sometimes too) hydrophobic.[52,53] In addition, PLA is chemically inert with few reactive centers, making surface and bulk modification a challenging task.[53] By introducing functional or adjustable chemical groups via homo- or copolymerization with lactic acid, access to different properties in (PLA-based) polyesters or anchor points for further modification can be obtained.[54] During the conversion of hemicellulosic sugars to lactates with Sn-based catalysts, traces of four-carbon α-hydroxy acid esters (C_4-AHAs), namely, methyl vinyl glycolate (MVG) and methyl-4-methoxy-2-hydroxybutanoate (MMHB), have been analyzed.[26,28,55] These compounds originate from tetrose sugars and glycolaldehyde (GA), the primary products of glucose retroaldol. In contrast, lactic acid or methyl lactate (MLA) originate from dihydroxyacetone (DHA) and glyceraldehyde (GLY), the two triose retroaldol products of fructose.

Received: June 26, 2015
Revised: August 20, 2015
Published: August 24, 2015

DOI: 10.1021/acscatal.5b01344
ACS Catal. 2015, 5, 5803−5811

Scheme 1. Schematic Representation of the Conversion of Glucose and Fructose to α-Hydroxy Acid Esters and Their Use As Functionalizable Polyester Building Units

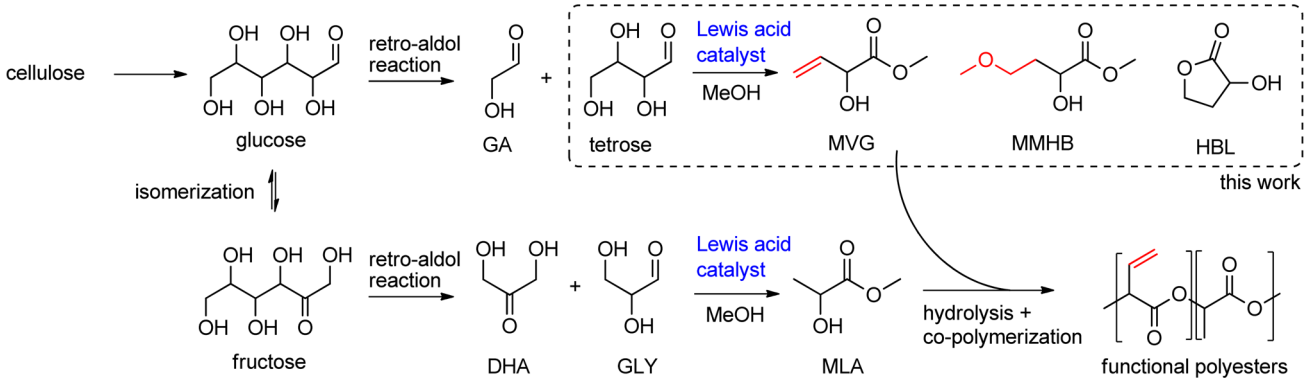

Copolymerization of functional C_4-AHAs with lactic acid can introduce functional groups in the PLA backbone, providing a possible solution for some of the current limitations of PLA (Scheme 1). As a proof of concept, our group successfully introduced up to 12% of vinyl glycolic acid (hydrolyzed version of MVG) in a PLA backbone.[56] Subsequently, the incorporated vinyl side groups in the polyester were found accessible to functionalization via thiol−ene chemistry. The hydrophilicity of the PLA-based polymer could be tuned by the choice of thiol via this approach.[56] We also elucidated the mechanistic details of C_4-AHA formation from tetroses[57] and glycolaldehyde[56] using homogeneous Sn halide catalysts in alcoholic media and showed that MMHB could be synthesized in one pot and in high yields at 363 K. However, (1) the selectivity toward MVG remained low and (2) homogeneous Sn catalysts are hard to recover for reuse. The use of solid Lewis acid catalysts could provide a more robust and environmentally sound solution for C_4-ester synthesis. Whereas the solid Lewis acid catalyzed conversion of trioses,[21−27,58−61] pentoses,[28] and hexoses[1,28,37,55] has been extensively reported, that of tetroses remains largely unexplored. Here, we systematically explore the conversion of tetrose sugars to C_4-AHAs in alcoholic media with solid Lewis acid catalysts. A selective route to MVG, the most versatile building block, is unraveled by tuning catalyst design and process parameters on the basis of insights in active site confinement effects.

EXPERIMENTAL SECTION

Catalysts. H-USY zeolites (CBV600, CBV712, and CBV720) and Al-β (CP814E) were purchased from Zeolyst international. The as-received catalysts were calcined in static air at 823 K (5 K min^{-1}) for 5 h prior to use to put the zeolites in their protonic form. Si-β was purchased from Tosoh (HSZ-980HOA, Si/Al = 255). SnO_2 was used as purchased (Alfa Aesar, <10 μm powder, 6 m^2 g^{-1}). SnO_2/Si-β was a physical mixture of SnO_2 and Si-β. Sn-, Ti-, and Zr-β;[62] Sn-β deAl;[1,31] Sn-MFI;[63] Sn-MCM-41;[24] and Sn-SBA-15[64] were synthesized according to methods known in the art. A more detailed description is given in the Supporting Information.

Characterization. Powder X-ray diffraction patterns were measured on a STOE Stadi P diffractometer using Cu $K\alpha_1$ radiation (λ = 0.154 nm) equipped with a Ge monochromator and image plate detector. Small-angle X-ray diffraction patterns (for Sn-MCM-41 and Sn-SBA-15) were measured on a SAXSess mc^2 instrument (Anton Paar) using line-collimated Cu Kα radiation and a 2D imaging plate detector. For elemental analysis, a Jeol Hyperprobe JXA-8530F field emission gun electron probe microanalyzer (FEG EPMA) equipped with five wavelength dispersive spectrometers (WDS) was used. Prior to conducting the measurement, powder-like samples were embedded in resin and allowed to harden. Then, the resin surface was ground, polished, and coated with carbon. The microprobe was operated at 15 kV and 50 nA. The Sn $L\alpha_1$-signal was detected using a PETH crystal. The Sn and Si content were quantified using a Cassiterite and Willemite standard, respectively. ZAF was used for the matrix correction method. Ten different spots were measured, and an average composition was calculated. N_2 physisorption measurements were performed on a Micromeritics Instruments Tristar 3000 at 77 K. All samples were degassed overnight at 673 K under a constant N_2 flow prior to analysis. Specific surface areas were calculated by the Brunauer−Emmett−Teller (BET) theory. Pore volumes were determined by the t-plot method on the desorption branch.

Catalytic Reactions. Reactions up to 363 K were performed in 10 mL thick-walled glass vial reactors. In a typical reaction, 2.5 mmol of (*S*)-(+)-erythrulose hydrate (97%, Sigma-Aldrich), 100 mg of catalyst, and 50 mg of internal standard (1,4-dioxane, Acros Organics) were weighed in a vial, and 5 mL of methanol and a magnetic stirring bar were added. The glass vials were closed by a crimp cap with a septum and placed in a multivial heating block, preset at the desired temperature (usually 363 K). Typically, the vials were allowed to react for 5 h under continuous stirring. Afterward, the vials were quenched in an ice bath. Reactions at temperatures over 363 K were performed in stainless steel pressurized batch reactors (12 mL) in the same manner, except for an additional triple N_2-flushing procedure, after which the reactor was filled with 20 bar of inert N_2. The pressurized reactors were placed in a preheated copper block at temperatures ranging from 393 to 433 K. After reaction and ice bath quenching to room temperature, excess pressure was released. All reaction mixtures were centrifuged at 3000 rpm for 5 min to separate the catalyst prior to analysis.

Analysis. MMHB and MVG were analyzed by GC−FID on a 30 m Agilent HP-5 column with N_2 as carrier gas. HBL was analyzed by GC−FID on a 30 m CP-SIL-5CB column with N_2 as carrier gas. Product yields were calculated with internal standards, taking into account the respective response factors for each compound as determined via calibration curves with commercial standards in the case of MVG (96%, TCI Europe) and HBL (>96%, TCI Europe) or by ECN-based calculations[65] for MMHB because of a lack of commercial standards. The conversion of erythrulose was determined by measuring the residual amount of erythrulose after reaction via HPLC (Agilent

DOI: 10.1021/acscatal.5b01344
ACS Catal. 2015, 5, 5803−5811

1200 Series). Residual amounts of other tetroses (i.e., threose and erythrose) were not taken into account. For this, 1 mL of reaction mixture was left to evaporate under a mild N_2 flow until a dry syrup was obtained. Then, 1 mL of Millipore water was added, and the solution was mixed and filtered over a 0.45 mm PTFE filter and analyzed on a Varian Metacarb 67C column (300 × 6.5 mm) equipped with a refractive index detector using Millipore water as the eluent. The conversion was calculated via a calibration curve of (*S*)-(+)-erythrulose hydrate (97%, Sigma-Aldrich). The column was kept at 358 K with a constant flow of 0.5 mL min^{-1}. Identification of compounds was performed by GC/MS with electronic ionization (Agilent 6890 series equipped with a 30 m HP-5MS capillary column with He as carrier gas), ^{13}C NMR, and by comparing GC retention times of the reaction mixture with dilute solutions of commercial standards of expected products.

RESULTS AND DISCUSSION

Catalyst Screening. Different Lewis acidic catalysts were tested for the conversion of erythrulose (ERU) in methanol at 363 K (Table 1). Three main products were identified by GC, GC/MS, and ^{13}C NMR (Supporting Information, Figure S1): MMHB, MVG, and α-hydroxy-γ-butyrolactone (HBL) (structures are shown in Scheme 1 and 2). The latter is a cyclic α-hydroxy acid that is an important intermediate in the production of herbicides and pharmaceutical compounds.[66,67] Erythrose and threose (tetrose isomerization) were detected in trace amounts. The proposed reaction mechanisms for C_4-AHA formation, in line with our earlier reports[56,57] and the work on a $C_1 + C_3$ aldol route toward HBL reported by Van de Vyver et al.,[20] are shown in Scheme 2. H-USY zeolites with different Si/Al ratios containing

Table 1. Catalyst Screening for the Conversion of ERU to C_4-AHAs[a]

			yield of C_4-esters (%)				
entry	catalyst	Si/M[b]	MVG	MMHB	HBL	total	conversion (%)
1	CBV600	2.6	<1	3	<1	3	95
2	CBV600[c]	2.6	2	11	2	15	77
3	CBV712	5.8	1	12	2	15	96
4	CBV720	15	<1	5	2	7	81
5	Al-β	12.5	<1	7	0	7	81
6	Ti-β	500[d]	4	17	3	24	58
7	Zr-β	500[d]	1	2	4	7	34
8	Sn-β	480	20	50	10	80	95
9	Sn-β[e]	480	19	52	8	79	88
10	Sn-β[f]	480	13	31	6	50	
11	Sn-β[g]	480	15	42	8	65	96
12	Sn-β deAl	62	24	47	5	76	93
13	SnO_2/Si-β	38[h]	0	0	0	0	37
14	SnO_2		1	0	0	1	7
15	Si-β (blank)		0	0	0	0	2
16	$SnCl_4 \cdot 5H_2O$[i]		2	53	4	59	96

[a]Conditions: 1.25 mmol ERU, 100 mg of catalyst, 5 mL of methanol, 50 mg of 1,4-dioxane, 363 K, 5 h reaction time. [b]Determined by manufacturer (in the case of H-USY) or by EPMA analysis. [c]Reaction temperature of 393 K. [d]Si/M ratio in the synthesis gel. [e]2.5 mmol of ERU. [f]4.17 mmol of ERU. [g]4.17 mmol of ERU, 20 h reaction time. [h]Calculated from the amount of SnO_2 and Si-β used. [i]2.5 mmol of ERU, 5 mol % catalyst; 10 mol % of catalyst yielded 76% of MMHB after 5 h.

Scheme 2. Proposed Reaction Scheme for the Conversion of Tetrose Sugars to C_4-AHAs

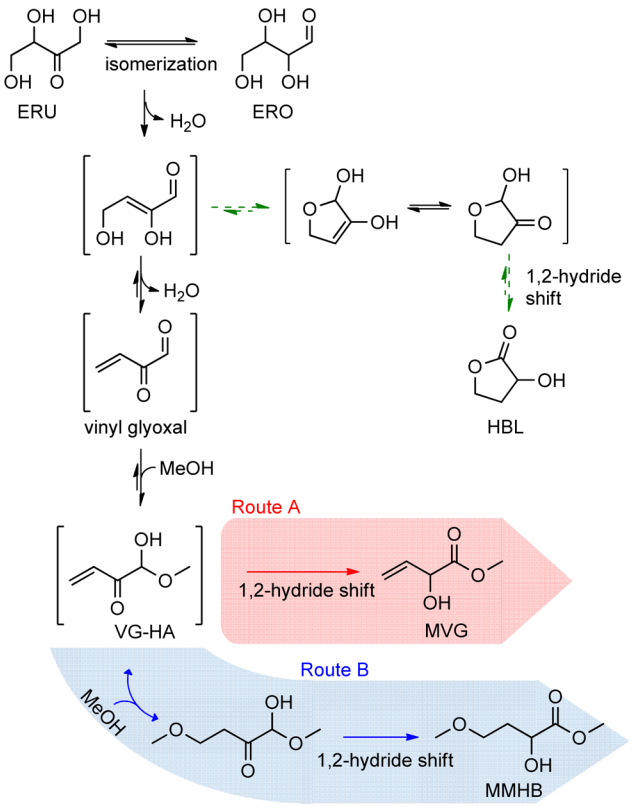

Lewis acidic extra-framework Al species yielded no significant amounts of C_4-esters (entries 1–4), in contrast to their reported activity for the conversion of trioses to alkyl lactates[21,22] and aqueous tetrose isomerizations.[7] A series of different β-zeolites containing Lewis acidic heteroatoms (Al, Ti, Zr, and Sn, entries 5–8) demonstrated the superior behavior of the Sn-β zeolite, yielding a combined 80% of C_4-AHA product at 95% conversion. This result exceeds the total yields obtained by using 5 mol % of homogeneous $SnCl_4 \cdot 5H_2O$ (entry 16). Because negative controls (Si-β, SnO_2, and SnO_2/Si-β, entries 13–15) yield no products, the activity of Sn-β can be attributed to the presence of highly dispersed Sn species in the framework, in agreement with the literature.[68−70] The Sn-β catalyst retains its conversion and selectivity levels, even when doubling the substrate loading (entry 9). Tripling the original substrate loading, however, results in a significant decrease in yield (entry 10). Although this might be due to an incomplete conversion, a prolonged reaction time only slightly increased the product yields (entry 11). Because the traditional bottom-up synthesis of Sn-β requires the use of fluoride media and long crystallization times (≥10 days), we also investigated the use of Sn-β prepared by a more accessible method, that is, by grafting Sn onto a dealuminated commercial β according to a procedure proposed by our group[1,31,71] (further denoted as Sn-β deAl). Its behavior matched that of the hydrothermal Sn-β (entry 12).

Time Profile. The catalytic action of Sn-β was monitored in time (Figure 1) and compared with literature values for homogeneous $SnCl_4 \cdot 5H_2O$.[57] The framework-incorporated Sn is more active than the dissolved Sn because the respective turnover frequencies (TOF, h^{-1}) were 330 $mol_{C4\text{-}AHA}$ mol_{Sn}^{-1} h^{-1} for Sn-β (calculated from the initial linear part of total C_4-ester yield, see Figure 1; and Si/M ratio from Table 2) versus ±54

DOI: 10.1021/acscatal.5b01344
ACS Catal. 2015, 5, 5803−5811

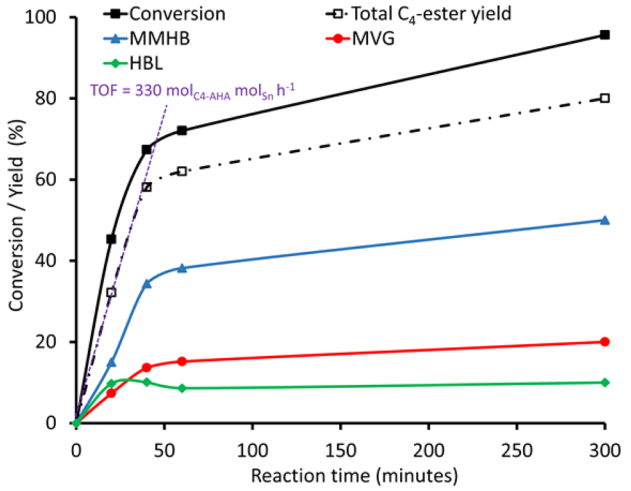

Figure 1. Conversion and yield as a function of time for a typical reaction of ERU (1.25 mmol) converted with Sn-β (100 mg) in methanol (5 mL) at 363 K.

$mol_{C4\text{-}AHA}\ mol_{Sn}^{-1}\ h^{-1}$ for the salt.[57] A similar trend, namely, a 10-fold increase, has been reported for the conversion of trioses to lactates.[61]

Influence of Pore Geometry on Product Selectivity. Remarkably, Sn incorporated in a zeolite matrix shows selectivity patterns different from those of soluble Sn: with $SnCl_4{\cdot}5H_2O$, MMHB is by far the major product (Table 1, entry 16), whereas Sn-β produces significant amounts of MVG and HBL, as well (Table 1, entry 8). We investigated if this was due to differences in Brønsted acidity in the reaction media, as dissolving $SnCl_4{\cdot}5H_2O$ in methanol potentially introduces strong Brønsted acidity due to Cl^- dissociation and in situ HCl formation.[56] When reacting ERU with Sn-β in methanol in the presence of 1 mol % HCl (relative to ERU), a strong decrease in product yields was noticed (8 and 3% for MMHB and MVG, respectively, after 1 h). Thus, the difference in selectivity does not seem to originate from differences in Brønsted acidity. Another explanation might be found in spatial limitations of the Sn active site inside the pores of the catalyst. Such a trend was observed earlier for the cyclization of citronellal into isopulegol, for which it was shown that the available space around the catalytic Lewis center had an influence on the diastereoselectivity of the reaction.[70,72] To assess whether similar effects could explain the selectivities in C_4-AHA formation, a series of solid Sn catalysts with varying pore sizes was synthesized for catalytic testing: Sn-MFI, Sn-β, Sn-MCM-41, and Sn-SBA-15. The MFI topology consists of a three-dimensional micropore system of 10-membered rings (5.5−6 Å) with straight channels interconnected by sinusoidal channels. The BEA topology contains 12-membered straight channels (6.6−6.7 Å, along axis [100]) interconnected by 12-membered zigzag channels (5.6 Å, along axis [001]).[73] MCM-41 and SBA-15, on the other hand, mainly consist of a regular arrangement of cylindrical mesopores in a hexagonal array but can also contain small amounts of micropores. Usually, mesopore diameters range from 2 to 6.5 nm and from 2 to 30 nm for MCM-41 and SBA-15 respectively, depending on their synthesis. The structures of MFI, β, and mesoporous silica are shown schematically in Figure 2.

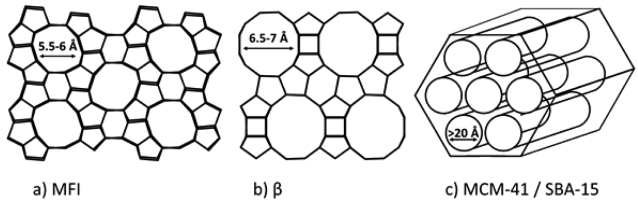

Figure 2. Schematic representation of the pore channels in (a) MFI, (b) β (BEA), and (c) mesoporous MCM-41 and SBA-15.

The catalysts were analyzed by powder-XRD and N_2-physisorption (Table 2) and compared with their fully siliceous analogues (Figures S2−S10). A high crystallinity was confirmed for Sn-β and Sn-MFI, and the presence of long-range order was verified for the mesoporous materials. The pore size distributions for Sn-MCM-41 and Sn-SBA-15 showed the presence of uniform mesopores with a pore width of 3.0 and 3.8 nm, respectively. For all materials, no diffraction lines corresponding to SnO_2 were observed. To verify a successful Sn incorporation, the catalytic activity of the series was asserted with the DHA to MLA reaction under the literature conditions (Table S1). All catalysts gave high MLA yields, proving the incorporation of catalytically active Sn species in the framework or silica walls.

The catalysts were then tested for the conversion of ERU to C_4-AHAs in methanol (Table 3). Sn-MCM-41 acquires high product yields after 5 h of reaction (entry 4), matching those of $SnCl_4{\cdot}5H_2O$, Sn-β, and Sn-β deAl (entries 1−3). The low activity of Sn-MFI (entry 5) could be due to diffusional limitations of the product or reagents in the narrow channels of the crystals, in agreement with empirical estimations of the kinetic molecule diameters compared with the zeolite pores (Table S2). Sn-SBA-15 is also less active than Sn-β or Sn-MCM-41 (entry 6), and triple catalyst loadings were required to match Sn-β yields after 5 h of reaction (entry 7). Interestingly, the product distributions

Table 2. Sample Composition and Physicochemical Characteristics of Different Heterogeneous Sn Catalysts

			BET surface area (m^2g^{-1})[c]			pore volume ($cm^3\ g^{-1}$)			
entry	catalyst	Si/M[a]	total	micropore[d]	mesopore[e]	total	micropore[d]	mesopore[e]	avg pore width[f] (Å)
1	Sn-MFI	269	444	428	0	0.19	0.19	0	5.5−6
2	Sn-β	480	550	542	0	0.23	0.23	0	6.6−6.7
3	Sn-β deAl	62	609	441	168	0.6	0.18	0.42[g]	6.6−6.7
4	Sn-MCM-41	36	960	35	925	0.69	0.008	0.69	30
5	Sn-SBA-15	50[b]	712	244	468	0.53	0.12	0.41	38

[a]Determined by EPMA analysis. [b]Si/M ratio in the synthesis gel (not determined by EPMA). [c]Ideally, the BET theory should not be applied to zeolites, but for literature comparison, the calculated BET surface areas for Sn-β, Sn-β deAl, and Sn-MFI are also given, albeit possibly underestimated.[74] [d]Determined using the *t*-plot method. [e]Calculated by subtracting the micropore surface area or pore volume from the total surface area or pore volume. [f]Values obtained from literature (for Sn-MFI and Sn-β) or from the pore size distributions (for Sn-MCM-41 and Sn-SBA-15). [g]The large mesopore volume is likely due to intercrystalline porosity/voids.[1]

DOI: 10.1021/acscatal.5b01344
ACS Catal. 2015, 5, 5803−5811

Table 3. Conversion of ERU to C_4-AHAs with Different Sn-Based Catalysts[a]

entry	catalyst	yield (%) MVG	MMHB	HBL	conv (%)
1	$SnCl_4{\cdot}5H_2O$[c]	2	53	4	96
2	Sn-β	20	50	10	95
3	Sn-β deAl	24	47	5	93
4	Sn-MCM-41	3	61	7	95
5	Sn-MFI[d]	9	12	8	87
6	Sn-SBA-15	3	26	6	79
7	Sn-SBA-15[e]	3	57	5	95
8	Sn-β[f]	33[f]	11[f]	8	86

[a]Conditions: 1.25 mmol of ERU, 100 mg of catalyst, 5 mL of methanol, 50 mg of 1,4-dioxane, 363 K, 5 h reaction time. [c]2.5 mmol of ERU, 5 mol % catalyst. [d]20 h reaction time. [e]300 mg of catalyst. [f]Reaction in ethanol for 20 h. Instead of MVG and MMHB, ethyl analogues of ethyl vinyl glycolate (EVG) and ethyl-4-ethoxy-2-hydroxy-butanoate (EEHB) are analyzed here.

with the mesoporous Sn-MCM-41 and Sn-SBA-15 catalysts are very similar to that of homogeneous $SnCl_4{\cdot}5H_2O$, with MMHB as the main product. As mentioned before, Sn-β produces significantly more MVG, even though MMHB is still the major product. Within the small pores of Sn-MFI, even more MVG and HBL are made relative to MMHB, albeit with lower total yields. The normalized product distributions in order of decreasing pore size (Figure 3) suggest a direct correlation between the pore size

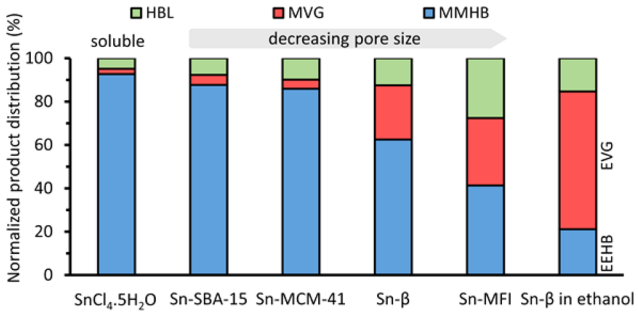

Figure 3. Influence of pore size of various Sn-based catalysts on the normalized C_4-AHA distribution in the conversion of ERU in methanol.

of the catalyst and the C_4-AHA product distribution. The selectivity to the bulkier MMHB increases with increasing pore sizes, whereas the selectivity to MVG and HBL increases with decreasing pore sizes.

These results suggest that confinement effects play a role in the reaction pathways (Scheme 2). A crucial intermediate that is assumed to largely influence the product selectivity in tetrose conversion[56,57] is the hemiacetal of vinyl glyoxal (VG-HA, Scheme 2). This intermediate can undergo two different reaction pathways, each resulting in a different final product: A direct 1,2-hydride shift of VG-HA produces MVG, trapping the vinyl bond in the final product (route A). On the other hand, if a methanol molecule is added to the terminal vinyl bond via a 1,4-nucleophilic addition prior to this 1,2-hydride shift, the final product is MMHB and the terminal vinyl group is replaced by a terminal methoxy group (route B).[57] Homogeneous $SnCl_4{\cdot}5H_2O$ and the mesoporous catalysts seem to prefer the latter route, probably because of the high reactivity of the vinyl group in conjugation with the carbonyl group in VG-HA. The spatial constrictions in the narrow channels of Sn-β and Sn-MFI might disturb this 1,4-nucleophilic addition, increasing the selectivity to MVG (and maybe HBL by equilibrium back-reactions). Such selectivity control shows the characteristics of transition-state shape selectivity, according to Weisz.[75]

A similar effect was recently discovered by Dusselier et al., who have noticed a great increase in selectivity toward lactide in the conversion of lactic acid using microporous H-β zeolites, compared with mesoporous or nonporous catalysts.[76] To further corroborate this hypothesis, we investigated the use of Sn-β in ethanol for forming the ethyl analogues ethyl vinyl glycolate (EVG) and ethyl-4-ethoxy-2-hydroxybutanoate (EEHB) from ERU. Previously, we noted that the use of ethanol slightly increased the selectivity to EVG (relative to EEHB) with $SnCl_4{\cdot}5H_2O$.[56,57] With Sn-β, however, the change in selectivity is far more pronounced in ethanol (Table 3, entry 8, and Figure 3). The lower nucleophilic strength of ethanol combined with the spatial limitations inside the pores significantly alters the product selectivity toward EVG. In ethanol with Sn-β, EEHB comprises only 21% of the total C_4-AHA fraction. This result is consistent with our hypothesis that differences in selectivity between homogeneous $SnCl_4{\cdot}5H_2O$ and porous heterogeneous catalysts are primarily due to a constraint active site inside the pores of the catalyst.

Influence of Temperature on Reaction Pathways. The influence of temperature on the product distribution was assessed with homogeneous $SnCl_4{\cdot}5H_2O$, mesoporous Sn-MCM-41, and Sn-SBA-15, and microporous Sn-β (Table 4). With $SnCl_4{\cdot}5H_2O$, no major differences are observed at higher reaction temperatures (even up to 433 K, entries 1–5). Sn-MCM-41 and Sn-SBA-15, on the other hand, show a slight increase in MVG and concomitant decrease in MMHB at higher temperatures (entries 6–15) with a maximum MVG yield of 10–

Table 4. Conversion of ERU to C_4-AHAs at Various Temperatures[a]

entry	catalyst	T (K)	yield (%) MVG	MMHB	HBL	conv (%)
1	$SnCl_4{\cdot}5H_2O$[b]	353	1	54	3	94
2		363	2	53	4	96
3		393	2	53	4	95
4		413	2	52	2	95
5		433[c]	7	57	3	96
6	Sn-MCM-41	353	2	52	4	94
7		363	3	61	7	>99
8		393	6	62	7	>99
9		413	10	60	8	>99
10		433[c]	10	44	6	>99
11	Sn-SBA-15[d]	353	2	49	5	95
12		363	3	57	4	92
13		393	7	50	5	94
14		413	10	46	5	95
15		433[c]	13	42	7	92
16	Sn-β	353	13	50	2	90
17		363	20	50	10	95
18		393	25	29	6	>99
19		413	34	20	7	>99
20		433[c]	50	18	8	>99

[a]Conditions: 1.25 mmol of ERU, 100 mg of catalyst, 5 mL of methanol, 50 mg of 1,4-dioxane, 5 h reaction time. [b]2.5 mmol of ERU, 5 mol % of catalyst. [c]Sample taken after 1 h reaction time to avoid product degradation. [d]300 mg of catalyst.

DOI: 10.1021/acscatal.5b01344
ACS Catal. 2015, 5, 5803–5811

13% at 433 K. The microporous Sn-β catalyst shows a more temperature-dependent selectivity pattern (entries 16−20): at lower reaction temperatures (353−363 K), MMHB is the major product (50% versus 13−20% of MVG), but at 393 K, Sn-β produces approximately equimolar amounts of MVG and MMHB. At the highest temperatures (413−433 K), the main product with Sn-β is MVG, with a yield up to 50% (versus 18% of MMHB). The latter result is in line with an earlier report stating that 56% of MVG was obtained when reacting erythrose with Sn-β in methanol at 433 K for 20 h.[55] The changing selectivities are strikingly visualized in the corresponding chromatograms of the reaction mixtures (Figure S11) and in Figure 4, which plots the

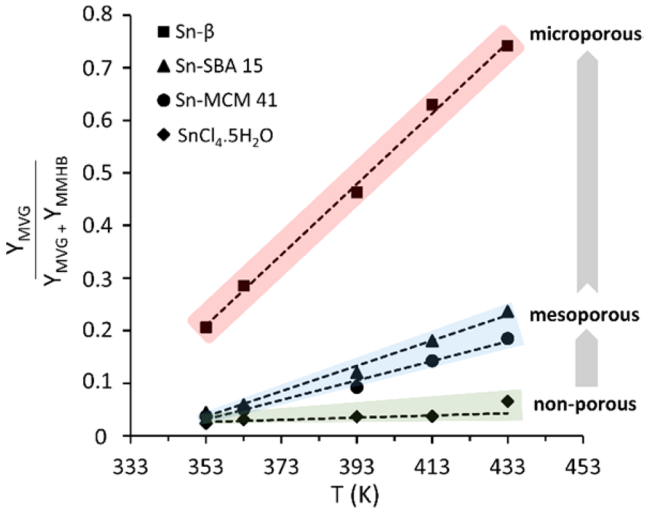

Figure 4. Influence of temperature on selectivity toward MVG, compared with the total amount of MVG and MMHB produced, for different Sn-based catalysts.

yields of MVG relative to the combined yields of MVG and MMHB. These results suggest that temperature alone has little to no isolated effect on the preferred reaction pathway; only in combination with confinement effects inside the pores of the heterogeneous catalyst is the selectivity altered.

Note that even though the mesopores of Sn-SBA-15 are slightly bigger than those of Sn-MCM-41, the product selectivity of the former is somewhat more sensitive to temperature. This might be due to the more pronounced presence of micropores in the SBA-15 structure (see Table 2, entries 4, 5). The postsynthetic Sn-β deAl behaved very similarly with changing temperature compared with hydrothermal Sn-β (Figure S12).

Kinetic Analysis. To further understand the selectivity changes at higher temperatures, a kinetic study was performed on the conversion of ERU with $SnCl_4{\cdot}5H_2O$, Sn-MCM-41, and Sn-β as representatives of for soluble, mesoporous, and microporous catalysts, respectively. Several reactions in the range of 353−373 K were carried out, and the product formation rates were determined from the initial, linear parts in the kinetic plots (details, see Figure S13) and used for the construction of Arrhenius plots (Figure 5 (left)). Note that average Si/M values were used to calculate the corresponding TOFs according to EPMA (Table 2), which might also include catalytically inactive Sn (e.g., Sn incorporated in the silica walls of Sn-MCM-41).

Apparent activation energies (E_a) for the formation of MVG and MMHB were derived from the slopes of these plots, whereas the pre-exponential factor k_0 (which is correlated to entropic factors, according to Eyring[77]) was derived from the calculated

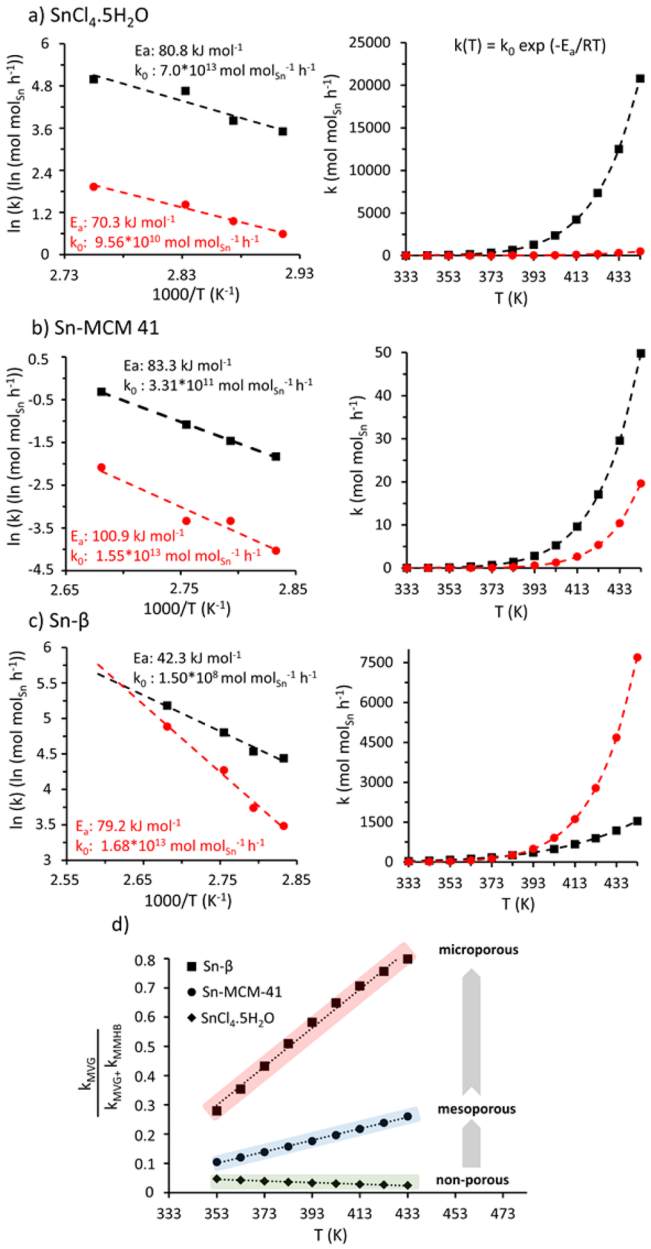

Figure 5. (a−c) Arrhenius plots of the conversion of ERU to MVG (red dots) and MMHB (black squares) with calculated activation energies and pre-exponential factors, k_0 (left), and accompanying rates of MVG and MMHB formation for different temperatures (right) for (a) $SnCl_4{\cdot}5H_2O$, (b) Sn-MCM-41, and (c) Sn-β. (d) Ratio of the initial rate at which MVG is formed relative to the initial production rate of MVG and MMHB combined (from the right side of parts a−c) as a function of the temperature.

intercept with the y-axis. Using the experimental values of E_a and k_0, a theoretical evolution of the reaction rate as a function of the reaction temperature was plotted for both compounds according to the formula $k = k_0 \exp(-E_a/RT)$ (Figure 5, right). For $SnCl_4{\cdot}5H_2O$, the formation of MMHB and MVG have comparable apparent activation energies (80.8 and 70.3 kJ mol^{-1}, respectively) but significantly different values for k_0, that is, that of MMHB is approximately a factor of 10^3 higher (Figure 5a, left). Therefore, despite similar activation energies, the rate of MMHB formation exceeds that of MVG at all calculated temperatures (Figure 5a, right).

DOI: 10.1021/acscatal.5b01344
ACS Catal. 2015, 5, 5803−5811

For the mesoporous Sn-MCM-41, the activation energy for MMHB remains about the same as for $SnCl_4 \cdot 5H_2O$ (83 kJ mol^{-1}), whereas that of MVG is higher (101 kJ mol^{-1}). However, here, k_0 for MVG formation slightly exceeds that of MMHB (approximately by a factor of 50; see Figure 5b, left). Although the rate of both compounds increases with increasing temperature, the rate of MVG formation does not exceed that of MMHB at the studied temperatures (Figure 5b, right).

The microporous Sn-β behaves very differently compared with $SnCl_4 \cdot 5H_2O$ or Sn-MCM-41. Here, MMHB formation has a much lower activation energy than the production of MVG (42.3 and 79.2 kJ mol^{-1}, respectively), but the value of k_0 for MVG significantly exceeds that of MMHB by a factor 10^5 (Figure 5c, left). The effect of such a high k_0 for MVG expresses itself in the model (Figure 5c right): at low temperatures (<393 K), the rate of MMHB formation is higher than that of MVG, whereas at high temperatures (>393 K), the rate of MVG increases quickly, eventually surpassing the rate of MMHB formation. These theoretical calculations of both reaction rates derived from k_0 and E_a correspond very well to our experimental observed product distributions. Indeed, Figure 5c (left) predicts an intersection point at 383 K, meaning that at this temperature, the rates of MVG and MMHB production with Sn-β should be equal. Close to this temperature, at 393 K, nearly equimolar yields of MVG and MMHB were obtained after 5 h (25 and 29% for MVG and MMHB, respectively; Table 4, entry 18).

Combined, the data suggest that the product selectivity for this reaction is kinetically controlled, that is, the product with the fastest production rate will be the favored product in the final mixture. To visualize this, we plotted the ratio of the initial rate at which MVG is formed relative to the total production rate of MVG and MMHB as a function of the temperature (Figure 5d). A clear similarity with the final product yield distribution shown in Figure 4 is noticed. The pre-exponential factor, k_0, is usually strongly correlated to entropic factors, which can be calculated through Eyring–Polanyi plots (Figure S14). From the slopes and intercepts of these plots, we calculated the entropy ($\Delta S^{\ddagger}$), enthalpy ($\Delta H^{\ddagger}$), and Gibbs energy ($\Delta G^{\ddagger}$) of activation for both products for different Sn catalysts (Table 5). Here, $\Delta S^{\ddagger}$ represents the change in entropy upon forming an activated transition state complex with the active site, which is generally correlated to changes in degrees of freedom (of translation, rotation, vibration). For $SnCl_4 \cdot 5H_2O$, the formation of MMHB is more entropically favored than MVG (10.4 versus −44.4 J mol^{-1} K^{-1}, respectively; a negative $\Delta S^{\ddagger}$ means a loss of entropy and, thus, a more ordered transition state complex). Using Sn-β, however, the formation of an activated complex toward MVG requires little loss in entropy (−1.7 J mol^{-1} K^{-1}), whereas the activation toward MMHB requires a strong decrease in entropy (−98.4 J mol^{-1} K^{-1}). This suggests that the active Sn site in the micropores of the Sn-β catalyst forms the required substrate orientation to convert VG-HA to MVG more efficiently than toward MMHB. This strongly indicates that steric hindrance inside the catalyst pores plays a dominant role in steering the preferred reaction route and, thus, also the product selectivity.

Table 5. Entropy ($\Delta S^{\ddagger}$), Enthalpy ($\Delta H^{\ddagger}$), and Gibbs Energy ($\Delta G^{\ddagger}$) of Activation for MVG and MMHB Formation with Different Sn Catalysts

		$SnCl_4 \cdot 5H_2O$	Sn-MCM-41	Sn-β
MVG	$\Delta S^{\ddagger a}$	−44.4	−2.3	−1.7
	$\Delta H^{\ddagger b}$	67.4	97.9	76.2
	$\Delta G^{\ddagger b,c}$	83.5	98.7	76.8
MMHB	$\Delta S^{\ddagger a}$	10.4	−34.3	−98.4
	$\Delta H^{\ddagger b}$	77.9	79.5	39.3
	$\Delta G^{\ddagger b,c}$	74.1	92.0	75.0

[a]Units: J mol^{-1} K^{-1}. [b]Units: kJ mol^{-1}. [c]Calculated at 363 K.

Although the interpretations made in this section are based on the assumption that true kinetics were measured, diffusional limitations for MMHB in Sn-β cannot be conclusively excluded. The apparent E_a of 42.3 kJ mol^{-1} with Sn-β is nearly half of the E_a calculated for the nonmicroporous catalysts (80.8–83.3 kJ mol^{-1}), which would be consistent with diffusionally limited transport inside the catalyst pores. Therefore, one could hypothesize that diffusional limitation of MMHB might steer the product selectivity toward MVG through product-type shape selectivity rather than transition state selectivity control. In that case, however, one would expect significant differences in the product distribution for different crystal sizes of Sn-β. Yet, similar results were obtained at different temperatures for the post-treated Sn-β deAl, of which the crystal sizes are orders of magnitude smaller than that of Sn-β synthesized in fluoride medium (approximately 10–30 nm vs 1–1.5 μm, respectively)[1] (Figure S12 and Table S3). This strongly suggests that the observed product selectivity of Sn-β is not governed by a physical phenomenon, but rather, by a chemical phenomenon such as active site confinement. Moreover, for Sn-β deAl, the E_a for MMHB formation is 57.2 kJ mol^{-1}, still less than for the nonmicroporous catalysts, but no longer following the $E_a/2$ rule (Figure S15). Similar to conventional Sn-β, a strong decrease in activation entropy (−71.0 J mol^{-1} K^{-1}) was noticed for MMHB (Figure S14). Thus, the results obtained with the much smaller Sn-β deAl crystals, in which the presence of diffusional limitations is less likely, are in line with our hypothesis of steering product selectivity through steric hindrance of the transition state around the Sn active site, in the absence of diffusional limitations.

Catalyst Recycling. Finally, we have assessed the reusability of the best-performing micro- and mesoporous catalysts, that is, Sn-β and Sn-MCM-41. For this, we performed five consecutive reactions with the same catalyst (which was separated from the reaction mixture via centrifugation) using an intermediate calcination step. The results are given in Figure 6, which shows that the Sn-β catalyst can be reused without significant losses in conversion or selectivities for 5 consecutive runs. For Sn-MCM-41, a slight decrease in the conversion is noticed, although total product yields did not change significantly after 5 runs.

CONCLUSIONS

Sn-based solid Lewis acids are highly active catalysts for the one-step conversion of tetrose sugars toward four-carbon α-hydroxy acid esters (C_4-AHA), useful as functional polyester building blocks. Sn incorporated in the zeolite matrix of Sn-β was significantly more active than soluble $SnCl_4 \cdot 5H_2O$, achieving an initial TOF of 330 $mol_{C4\text{-}AHA}$ mol_{Sn}^{-1} h^{-1}, as compared with ±54 $mol_{C4\text{-}AHA}$ mol_{Sn}^{-1} h^{-1}, respectively. We have shown that Lewis acid confinement effects strongly control the product selectivity, that is, microporous Sn catalysts produce significantly more MVG than mesoporous or soluble catalysts, which favor MMHB formation. This effect can be further magnified at higher reaction temperatures. By increasing the temperature from 353 to 433 K using a Sn-β catalyst, the MVG yield could be increased from 20% to 50%. It is likely that, in microporous catalysts, the formation of MMHB is sterically hampered inside the catalyst

DOI: 10.1021/acscatal.5b01344
ACS Catal. 2015, 5, 5803–5811

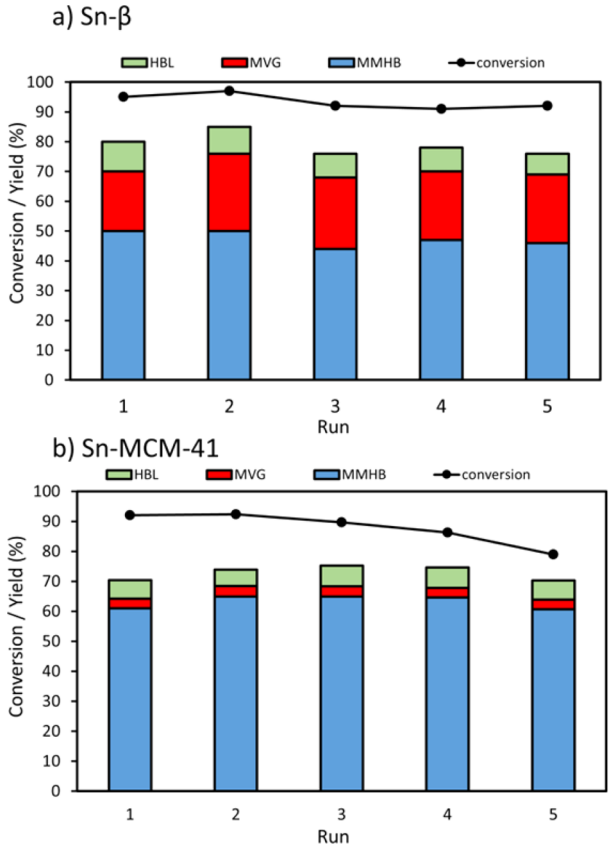

Figure 6. Recycling of (a) Sn-β and (b) Sn-MCM-41 catalysts for the conversion of ERU to C_4-AHAs. Reaction conditions: 1.25 mmol of ERU, 100 mg of catalyst, 50 mg of 1,4-dioxane, 5 mL of methanol, 363 K, 5 h reaction time.

pores, relatively steering the preferred reaction route, from the same precursor, toward MVG. The latter is the most desired monomer for versatile polyester chemistry. Moreover, the product selectivity seems to be under kinetic control. Finally, the best-performing micro- and mesoporous catalysts, namely, Sn-β and Sn-MCM-41, could be successfully reused for five consecutive runs.

■ ASSOCIATED CONTENT

Supporting Information

The Supporting Information is available free of charge on the ACS Publications website at DOI: 10.1021/acscatal.5b01344.

Catalyst preparation, ^{13}C NMR spectra of the reaction mixture, powder XRD patterns, N_2-physisorption isotherms and pore size distributions, GC chromatograms after reaction at various temperatures, kinetic plots to draft the Arrhenius plots, Eyring–Polanyi plots, results of DHA conversion to MLA, a comparison of estimated kinetic diameters of molecules to catalyst pore sizes, and results of ERU conversion with Sn-β deAl at various temperatures (PDF)

■ AUTHOR INFORMATION

Corresponding Authors

*E-mail: michiel.dusselier@biw.kuleuven.be.
*E-mail: bert.sels@biw.kuleuven.be.

Present Address

[§]Chemical engineering, California institute of Technology, Pasadena, California 91125, United States

Notes

The authors declare no competing financial interest.

■ ACKNOWLEDGMENTS

R.D.C. thanks IWT (Agency for Innovation by Science and Technology, project number 131404) for financial support. M.D. acknowledges FWO Vlaanderen for postdoctoral funding and the Belgian American Educational Foundation (BAEF) for his honorary fellowship. M.D. and B.F.S thank the Research Counsil of KU Leuven, IDO KP/14/003. The EPMA-WDS work has been feasible due to the support of the Hercules Foundation (project ZW09-09). We thank professor Johan Martens and Stef Kerkhofs for measurement of small-angle X-ray diffraction patterns.

■ REFERENCES

(1) Dijkmans, J.; Gabriëls, D.; Dusselier, M.; de Clippel, F.; Vanelderen, P.; Houthoofd, K.; Malfliet, A.; Pontikes, Y.; Sels, B. F. *Green Chem.* **2013**, *15*, 2777–2785.
(2) Román-Leshkov, Y.; Moliner, M.; Labinger, J. a.; Davis, M. E. *Angew. Chem.* **2010**, *122*, 9138–9141.
(3) Choudhary, V.; Pinar, A. B.; Sandler, S. I.; Vlachos, D. G.; Lobo, R. F. *ACS Catal.* **2011**, *1*, 1724–1728.
(4) Choudhary, V.; Caratzoulas, S.; Vlachos, D. G. *Carbohydr. Res.* **2013**, *368*, 89–95.
(5) Moliner, M.; Román-Leshkov, Y.; Davis, M. E. *Proc. Natl. Acad. Sci. U. S. A.* **2010**, *107*, 6164–6168.
(6) Saravanamurugan, S.; Paniagua, M.; Melero, J. A.; Riisager, A. *J. Am. Chem. Soc.* **2013**, *135*, 5246–5249.
(7) Saravanamurugan, S.; Riisager, A. *Catal. Sci. Technol.* **2014**, *4*, 3186–3190.
(8) Lew, C. M.; Rajabbeigi, N.; Tsapatsis, M. *Microporous Mesoporous Mater.* **2012**, *153*, 55–58.
(9) Wolf, P.; Hammond, C.; Conrad, S.; Hermans, I. *Dalt. Trans.* **2014**, *43*, 4514–4519.
(10) Chang, C.-C.; Wang, Z.; Dornath, P.; Je Cho, H.; Fan, W. *RSC Adv.* **2012**, *2*, 10475.
(11) Corma, A.; Domine, M. E.; Valencia, S. *J. Catal.* **2003**, *215*, 294–304.
(12) Lewis, J. D.; Van de Vyver, S.; Crisci, A. J.; Gunther, W. R.; Michaelis, V. K.; Griffin, R. G.; Román-Leshkov, Y. *ChemSusChem* **2014**, *7*, 2255–2265.
(13) Luo, H. Y.; Consoli, D. F.; Gunther, W. R.; Román-Leshkov, Y. *J. Catal.* **2014**, *320*, 198–207.
(14) Corma, A.; Domine, M. E.; Nemeth, L.; Valencia, S. *J. Am. Chem. Soc.* **2002**, *124*, 3194–3195.
(15) Moliner, M. *Dalt. Trans.* **2014**, *43*, 4197–4208.
(16) Corma, A.; Navarro, M. T.; Renz, M. *J. Catal.* **2003**, *219*, 242–246.
(17) Corma, a; Nemeth, L. T.; Renz, M.; Valencia, S. *Nature* **2001**, *412*, 423–425.
(18) Assary, R. S.; Curtiss, L. A. *J. Phys. Chem. A* **2011**, *115*, 8754–8760.
(19) Bermejo-Deval, R.; Assary, R. S.; Nikolla, E.; Moliner, M.; Román-Leshkov, Y.; Hwang, S.-J.; Palsdottir, A.; Silverman, D.; Lobo, R. F.; Curtiss, L. A.; Davis, M. E. *Proc. Natl. Acad. Sci. U. S. A.* **2012**, *109*, 9727–9732.
(20) Van de Vyver, S.; Odermatt, C.; Romero, K.; Prasomsri, T.; Roman-Leshkov, Y. *ACS Catal.* **2015**, *5*, 972–977.
(21) Pescarmona, P. P.; Janssen, K. P. F.; Delaet, C.; Stroobants, C.; Houthoofd, K.; Philippaerts, A.; De Jonghe, C.; Paul, J. S.; Jacobs, P. a.; Sels, B. F. *Green Chem.* **2010**, *12*, 1083–1089.

DOI: 10.1021/acscatal.5b01344
ACS Catal. 2015, 5, 5803–5811

(22) West, R. M.; Holm, M. S.; Saravanamurugan, S.; Xiong, J.; Beversdorf, Z.; Taarning, E.; Christensen, C. H. *J. Catal.* **2010**, *269*, 122−130.
(23) Li, L.; Collard, X.; Bertrand, A.; Sels, B. F.; Pescarmona, P. P.; Aprile, C. *J. Catal.* **2014**, *314*, 56−65.
(24) Li, L.; Stroobants, C.; Lin, K.; Jacobs, P. A.; Sels, B. F.; Pescarmona, P. P. *Green Chem.* **2011**, *13*, 1175−1181.
(25) Guo, Q.; Fan, F.; Pidko, E.; van der Graaff, W. N. P.; Feng, Z.; Li, C.; Hensen, E. J. M. *ChemSusChem* **2013**, *6*, 1352−1356.
(26) De Clippel, F.; Dusselier, M.; Van Rompaey, R.; Vanelderen, P.; Dijkmans, J.; Makshina, E.; Giebeler, L.; Oswald, S.; Baron, G. V.; Denayer, J. F. M.; Pescarmona, P. P.; Jacobs, P. a; Sels, B. F. *J. Am. Chem. Soc.* **2012**, *134*, 10089−10101.
(27) Dapsens, P. Y.; Kusema, B. T.; Mondelli, C.; Pérez-Ramírez, J. *J. Mol. Catal. A: Chem.* **2014**, *388*−*389*, 141−147.
(28) Holm, M. S.; Pagán-Torres, Y. J.; Saravanamurugan, S.; Riisager, A.; Dumesic, J.; Taarning, E. *Green Chem.* **2012**, *14*, 702−706.
(29) Dapsens, P. Y.; Menart, M. J.; Mondelli, C.; Pérez-Ramírez, J. *Green Chem.* **2014**, *16*, 589−593.
(30) Dapsens, P. Y.; Mondelli, C.; Pérez-Ramírez, J. *ChemSusChem* **2013**, *6*, 831−839.
(31) Dijkmans, J.; Dusselier, M.; Gabriëls, D.; Houthoofd, K.; Magusin, P.; Huang, S.; Pontikes, Y.; Trekels, M.; Vantomme, A.; Giebeler, L.; Oswald, S.; Sels, B. F. *ACS Catal.* **2015**, *5*, 928−940.
(32) Tolborg, S.; Sádaba, I.; Osmundsen, C. M.; Fristrup, P.; Holm, M. S.; Taarning, E. *ChemSusChem* **2015**, *8*, 613−617.
(33) Cho, H. J.; Chang, C.-C.; Fan, W. *Green Chem.* **2014**, *16*, 3428−3433.
(34) Bozell, J. J.; Petersen, G. R. *Green Chem.* **2010**, *12*, 539−554.
(35) Dusselier, M.; Sels, B.; In *Topics in Current Chemistry*; Nicholas, K. M., Ed.; Springer: Berlin Heidelberg, 2014; Vol. *353*, p 85−125.
(36) Dusselier, M.; Mascal, M.; Sels, B. F. In *Topics in current chemistry*; Nicholas, K. M., Ed.; Springer: Berlin Heidelberg, 2014; Vol. *353*, p 1−40.
(37) Dusselier, M.; Van Wouwe, P.; Dewaele, A.; Makshina, E.; Sels, B. F. *Energy Environ. Sci.* **2013**, *6*, 1415−1442.
(38) Fan, Y.; Zhou, C.; Zhu, X. *Catal. Rev.: Sci. Eng.* **2009**, *51*, 293−324.
(39) Schutyser, W.; Koelewijn, S.-F.; Dusselier, M.; Van de Vyver, S.; Thomas, J.; Yu, F.; Carbone, J. M.; Smet, M.; Van Puyvelde, P.; Dehaen, W.; Sels, B. F. *Green Chem.* **2014**, *16*, 1999−2007.
(40) Pereira, C. S. M.; Silva, V. M. T. M.; Rodrigues, A. E. *Green Chem.* **2011**, *13*, 2658−2671.
(41) Henton, D. E.; Gruber, P.; Lunt, J.; Randall, Jed. In *Natural Fibers, Biopolymers and Biocomposites*; Mohanty, A. K., Misra, M., Drzal, L., Eds.; CRC Press: Boca Raton, FL, 2005; p 527−578.
(42) Inkinen, S.; Hakkarainen, M.; Albertsson, A.-C.; Södergård, A. *Biomacromolecules* **2011**, *12*, 523−532.
(43) Law, K. L.; Thompson, R. C. *Science* **2014**, *345*, 144−145.
(44) Thompson, R. C.; Olsen, Y.; Mitchell, R. P.; Davis, A.; Rowland, S. J.; John, A. W. G.; McGonigle, D.; Russell, A. E. *Science* **2004**, *304*, 838.
(45) Law, K. L.; Morét-Ferguson, S.; Maximenko, N. A.; Proskurowski, G.; Peacock, E. E.; Hafner, J.; Reddy, C. M. *Science* **2010**, *329*, 1185−1188.
(46) Woodall, L. C.; Sanchez-vidal, A.; Canals, M.; Paterson, G. L. J.; Coppock, R.; Sleight, V.; Calafat, A.; Rogers, A. D.; Narayanaswamy, B. E.; Thompson, R. C. *R. Soc. Open Sci.* **2014**, *1*, 1−8.
(47) Cózar, A.; Echevarría, F.; González-Gordillo, J. I.; Irigoien, X.; Úbeda, B.; Hernández-León, S.; Palma, Á. T.; Navarro, S.; García-de-Lomas, J.; Ruiz, A.; Fernández-de-Puelles, M. L.; Duarte, C. M. *Proc. Natl. Acad. Sci. U. S. A.* **2014**, *111*, 10239−10244.
(48) Gilding, D. K.; Reed, A. M. *Polymer* **1979**, *20*, 1459−1464.
(49) Nair, L. S.; Laurencin, C. T. *Prog. Polym. Sci.* **2007**, *32*, 762−798.
(50) Rancan, F.; Papakostas, D.; Hadam, S.; Hackbarth, S.; Delair, T.; Primard, C.; Verrier, B.; Sterry, W.; Blume-Peytavi, U.; Vogt, A. *Pharm. Res.* **2009**, *26*, 2027−2036.
(51) Auras, R., Lim, L.-T., Selke, S. E. M., Tsuji, H., Eds.; *Poly(Lactic Acid): Synthesis, Structures, Properties, Processing, and Applications*; John Wiley & Sons Inc.: New York, 2010.
(52) Drumright, R. E.; Gruber, P. R.; Henton, D. E. *Adv. Mater.* **2000**, *12*, 1841−1846.
(53) Rasal, R. M.; Janorkar, A. V.; Hirt, D. E. *Prog. Polym. Sci.* **2010**, *35*, 338−356.
(54) Tian, H.; Tang, Z.; Zhuang, X.; Chen, X.; Jing, X. *Prog. Polym. Sci.* **2012**, *37*, 237−280.
(55) Holm, M. S.; Saravanamurugan, S.; Taarning, E. *Science* **2010**, *328*, 602−605.
(56) Dusselier, M.; Van Wouwe, P.; De Smet, S.; De Clercq, R.; Verbelen, L.; Van Puyvelde, P.; Du Prez, F. E.; Sels, B. F. *ACS Catal.* **2013**, *3*, 1786−1800.
(57) Dusselier, M.; Van Wouwe, P.; de Clippel, F.; Dijkmans, J.; Gammon, W.; Sels, B. F. *ChemCatChem* **2013**, *5*, 569−575.
(58) Osmundsen, C. M.; Holm, M. S.; Dahl, S.; Taarning, E. *Proc. R. Soc. London, Ser. A* **2012**, *468*, 2000−2016.
(59) Janssen, K. P. F.; Paul, J. S.; Sels, B. F.; Jacobs, P. a. *Stud. Surf. Sci. Catal.* **2007**, *170*, 1222−1227.
(60) Wang, J.; Masui, Y.; Onaka, M. *Appl. Catal., B* **2011**, *107*, 135−139.
(61) Taarning, E.; Saravanamurugan, S.; Spangsberg Holm, M.; Xiong, J.; West, R. M.; Christensen, C. H. *ChemSusChem* **2009**, *2*, 625−627.
(62) Zhang, X.; Kang, Z.; Liu, H.; Qiu, J. Method for synthesizing heteroatom Sn-beta zeolite. CN102249258 A, November 23, 2011.
(63) Mal, N. K.; Ramaswamy, V.; Rajamohanan, P. R.; Ramaswamy, A. V. *Microporous Mater.* **1997**, *12*, 331−340.
(64) Ramaswamy, V.; Shah, P.; Lazar, K.; Ramaswamy, a. V. *Catal. Surv. Asia* **2008**, *12*, 283−309.
(65) Scanlon, J. T.; Willis, D. E. *J. Chromatogr. Sci.* **1985**, *23*, 333−340.
(66) Mulzer, J.; Mantoulidis, A.; Öhler, E. *J. Org. Chem.* **2000**, *65*, 7456−7467.
(67) Kagayama, T.; Sakaguchi, S.; Ishii, Y. *Tetrahedron Lett.* **2005**, *46*, 3687−3689.
(68) Boronat, M.; Concepción, P.; Corma, A.; Renz, M.; Valencia, S. *J. Catal.* **2005**, *234*, 111−118.
(69) Boronat, M.; Corma, A.; Renz, M.; Viruela, P. M. *Chem. - Eur. J.* **2006**, *12*, 7067−7077.
(70) Boronat, M.; Concepcion, P.; Corma, A.; Navarro, M. T.; Renz, M.; Valencia, S. *Phys. Chem. Chem. Phys.* **2009**, *11*, 2876−2884.
(71) Dijkmans, J.; Demol, J.; Houthoofd, K.; Huang, S.; Pontikes, Y.; Jacobs, P.; Sels, B. F. *J. Catal.* **2015**, DOI: 10.1016/j.jcat.2015.06.023.
(72) Boronat, M.; Corma, A.; Renz, M. In *Turning Points in Solid-State, Materials and Surface Science*; Harris, K. D. M., Edwards, P. P., Eds.; The Royal Society of Chemistry: Cambridge, UK, 2008; pp 639−650.
(73) Bárcia, P. S.; Silva, J. a. C.; Rodrigues, A. E. *Microporous Mesoporous Mater.* **2005**, *79*, 145−163.
(74) Bae, Y.-S.; Yazaydın, a. O.; Snurr, R. Q. *Langmuir* **2010**, *26*, 5475−5483.
(75) Weisz, P. B. *Pure Appl. Chem.* **1980**, *52*, 2091−2103.
(76) Dusselier, M.; Van Wouwe, P.; Dewaele, A.; Sels, B. F. *Science* **2015**, *349*, 78−80.
(77) Eyring, H. *J. Chem. Phys.* **1935**, *3*, 107−115.

DOI: 10.1021/acscatal.5b01344
ACS Catal. 2015, 5, 5803−5811